AIAA JOURNAL
Vol. 31, No. 2, February 1993

Higher-Order Accuracy for Upwind Methods by Using the Compatibility Equations

Peter M. Goorjian* and Shigeru Obayashi†
NASA Ames Research Center, Moffett Field, California 94035

A new algorithm has been developed for obtaining higher-order accuracy in upwind schemes for the Euler and Navier-Stokes equations. In this method, the compatibility relations for the Euler equations are used to construct formulas for the higher-order interpolates. By using these formulas, computed results are obtained for steady, inviscid flow through a nozzle and also steady, inviscid, and viscous flow over an airfoil. This approach provides an alternative to total-variation-diminishing and essentially nonoscillatory schemes.

I. Introduction

ACCURATE calculations of flows that use upwind algorithms[1,2] require that the first-order scheme be extended to higher-order accuracy. The two well-known methods[3] used for higher-order accuracy are total-variation-diminishing (TVD)[4] and essentially nonoscillatory (ENO) schemes.[5] In this paper, a new method is presented[6] that uses the compatibility relations for the Euler equations to construct formulas for the higher-order interpolates. It achieves higher-order accuracy while maintaining nonoscillatory behavior in the solutions. This method does not use either the limiter functions of TVD schemes or the data-dependent computational stencils of ENO schemes. For the calculations in this paper, the formulas were implemented in a monotonic upstream schemes for conservation laws (MUSCL) scheme.

There is other work in which higher-order accuracy is achieved without the use of the techniques in either TVD or ENO schemes. For example, Roe[1] has developed a first-order upwind scheme with upwind-biased source terms that is monotonic and second-order accurate in the steady state. This scheme has been used for flow through a nozzle.[7] However, this scheme applies only to one-dimensional equations. Another example is the method developed by Lerat and Sides,[8] which uses a centered implicit scheme. This method is second-order accurate and does not use either artificial viscosity or upwinding. However, neither of these methods uses the compatibility equations to achieve higher-order accuracy.

The objective of this research is to develop a method for achieving higher-order accuracy in upwind schemes that is based on the physics of the flow field. The physics is provided by the wave structures in the flow, such as the entropy waves, the acoustic waves, and the vorticity waves. Each of these physical waves is manifested in the Euler equations by a corresponding compatibility relation (i.e., compatibility equation). Just as these compatibility equations have been used to develop first-order upwind algorithms, here they will be used to develop formulas for the higher-order interpolates. Hence, this approach for higher-order accuracy is consistent in approach with the development of the underlying first-order upwind schemes and can be used with any upwind scheme.

The physics of the flow field is again used to maintain nonoscillatory behavior at transonic shock waves. The Mach number component passes through one across the shock waves. Hence, transonic shock wave discontinuities are located by the vanishing of eigenvalues in the compatability relations for the acoustic waves. This approach is used in upwind schemes and it will be employed here in developing a higher-order algorithm. For comparison, this approach is fundamentally different from the method used by limiter functions or ENO schemes. In those schemes, discontinuities are located at extrema that are determined by comparing adjacent gradients in flow variables. However, not all extrema are the locations of discontinuities. For example, in multidimensional flow, extrema along coordinate lines will occur in smooth regions of the flow in the neighborhoods of vortices or stagnation points. The use of limiter functions at such extrema can effectively add numerical dissipation to the calculations and thereby reduce the resultant accuracy.

To gain a perspective on the new method, the essential ideas of previous methods to control numerical oscillatory behavior are examined next. Central differencing schemes[9] employ blended second- and fourth-order numerical dissipation operators, which are data processing procedures for suppressing the numerical oscillations. Such operators are derived from the heat equation and do not employ the wave structure of the flow field. In fact, these operators damp wave structures, such as shock waves and contact surfaces. Also TVD schemes that use limiter functions and ENO schemes use general mathematical procedures for data processing to control discontinuities. Such procedures are used for many purposes, such as image enhancement. However, none of those methods use the wave structures of the flowfield as embodied in the compatibility equations.

The idea of using the compatibility equations to achieve nonoscillatory solutions in higher-order upwind methods was first introduced[10] for calculations that used the transonic, small-disturbance equation. In that paper, calculations were shown for steady and unsteady, transonic and supersonic flows over airfoils. The method extended the standard first-order scheme in the supersonic regions to second-order and the results were nonoscillatory. The comparisons showed marked improvements in resolving the shock waves in both steady and unsteady calculations.

In Sec. II of this paper, the basic idea of using compatibility equations will be illustrated with the linear advection equation. Also, the monotonicity property will be proven for the method. Then for the Euler equations, formulas will be derived for higher-order interpolates, which will again use the compatibility equations.

Received May 9, 1991; presented as Paper 91-1543 at the AIAA 10th Computational Fluid Dynamics Conference, Honolulu, HI, June 24-26, 1991; revision received June 29, 1992; accepted for publication July 6, 1992.

*Research Scientist. Associate Fellow AIAA.
†Senior Research Scientist, MCAT Institute, San Jose, CA 95127. Senior Member AIAA.

In Sec. III, results from several test calculations are illustrated. First, solutions are given for Burger's equation with a source term. Next, solutions of Euler's equations for flow through a converging and diverging nozzle are shown. Then results from flow over an airfoil are offered. Both cases of subsonic and supersonic freestreams are presented for inviscid flow. Finally, results for viscous flow in the subsonic case are shown. The results indicate that higher-order spatial accuracy can be achieved by using the compatibility equations.

II. Numerical Algorithm

Linear Advection Equation

Consider the linear advection equation

$$u_t + au_x = 0, \qquad a > 0 \tag{1}$$

For this model equation, Eq. (1) is both the governing equation in conservation form for the conserved variable u and the compatibility equation for the characteristic variable u. For Euler's equations, the equations in conservation form are different than the compatibility equations. The standard, explicit, first-order, upwind, finite-difference algorithm for Eq. (1) is given[1] by

$$u_j^{n+1} = u_j^n - \nu \nabla u_j^n \tag{2}$$

where

$$\nabla u_j = u_j - u_{j-1}, \qquad \nu = a\Delta t/\Delta x, \qquad \nu \le 1 \tag{3}$$

In Eq. (2), the cell interface flux at $j+1/2$ is u_j^n, which is a first-order accurate flux evaluation. Furthermore, in Eq. (2) the coefficients of u_j^n and u_{j-1}^n are $(1-\nu)$ and ν, respectively. Hence for $\nu \le 1$, the algorithm is monotonic.

The idea in Ref. 10 is used again here to achieve higher-order accuracy in the interpolation for the spatial cell interface fluxes. Following the development of Ref. 10, a linear combination of Eq. (2) taken from mesh points j and $j-1$ with weights 3/2 and $-1/2$, respectively, is formed. The reason to form a linear combination of all the equations taken from different mesh points, including the time derivatives, is that the resulting equation is again a monotone scheme, as will be proven in the next section. The resulting equation is given by

$$(u_j^{n+1} + \tfrac{1}{2}\nabla u_j^{n+1}) = (u_j^n + \tfrac{1}{2}\nabla u_j^n) - \nu \nabla (u_j^n + \tfrac{1}{2}\nabla u_j^n) \tag{4}$$

In Eq. (4), the cell interface flux at $j+1/2$ is $u_j^n + (u_j^n - u_{j-1}^n)/2$, which is a second-order accurate flux evaluation. Another way to regard the construction of Eq. (4) is that u_j has been replaced with $u_j + (u_j - u_{j-1})/2$ for each term that occurs in Eq. (2), including those that have originated in the discretization of the time derivative. In Eq. (4), although the spatial flux evaluation is second-order accurate, the temporal difference now has a first-order spatial error, so the overall algorithm in space and time is still only first-order accurate. However, for equations with either source terms or for equations in multidimensions, these techniques will provide steady solutions with second-order accuracy, as will be shown.

Equation (4) may also be equivalently derived from Eq. (2) by the procedure of replacing the first-order cell interface flux u_j^n in Eq. (2) at location $j+1/2$ with the term

$$u_{j+1/2}^n = u_j^n + \tfrac{1}{2}\left[\nabla u_j^n + (1/\nu)(u_j^{n+1} - u_j^n)\right] \tag{5}$$

In Eq. (5), the addition of the part in brackets provides a term for the second-order spatial interpolate and also adds a temporal difference term. The term in brackets is derived from the left-hand side of the compatibility equation, Eq. (1), including the time derivative. The use of the compatibility equation distinguishes this method from limiter functions and ENO formulas. For the Euler equations, formulas similar in form to Eq. (5) will be derived for the primitive variables to provide higher-order interpolates, which will be used in the flux terms.

Stability Properties

A standard linear stability analysis has been performed on Eq. (4) and also for the case when the spatial fluxes are evaluated implicitly. The resulting growth factors are found to be identical to those for Eq. (2). Hence, the stability limit is $\nu \le 1$ for explicit spatial fluxes and no limit exists for implicit spatial fluxes.

Equation (4) is a monotone algorithm, which can be seen as follows. Equation (4) at mesh point j has been formed by taking a linear combination of equations of the form of Eq. (2) at mesh points j and $j-1$. The system of equations at all J mesh points, as given by Eq. (4), represents a linear system of J equations in J unknowns. Each equation of that system couples two of the unknowns, that is, u_j^{n+1} and u_{j-1}^{n+1}. Equation (2) gives the unique solution to that system of equations. In other words, the solution to Eq. (4) also satisfies Eq. (2). However, Eq. (2) is the standard, first-order upwind algorithm, which is known to be monotonic. Therefore, Eq. (4) is also monotonic since its solution is also the solution to a monotonic equation.

Also, Eq. (4) is like Eq. (2) in being first-order accurate in space. However, the first-order spatial error in Eq. (4) has the form $(\Delta x)u_{xt}$, which means that at steady state the first-order spatial error vanishes. The term u_{xt} is what distinguishes this method from other higher-order methods, such as the standard limiter function and ENO schemes. Here the space and time discretization are linked together, since the full compatibility equations are used. For comparison, other methods only modify the spatial discretization.

Euler Equations

In this section, the compatibility relations for the Euler equations will be used to obtain formulas for higher-order interpolates of the primitive variables. The compatibility equations in one dimension are given by

$$\left[\rho_t - (1/a^2)p_t\right] + u\left[\rho_x - (1/a^2)p_x\right] = 0 \tag{6}$$

$$(p_t + \rho a u_t) + (u+a)(p_x + \rho a u_x) = 0 \tag{7}$$

$$(p_t - \rho a u_t) + (u-a)(p_x - \rho a u_x) = 0 \tag{8}$$

Equation (6) is the equation for the entropy wave and Eqs. (7) and (8) are those for the two acoustic waves. Discretization of these equations will provide formulas for the spatial increments ∇p_j^n, $\nabla \rho_j^n$, and ∇u_j^n, which will be used for higher-order interpolates. Equations (6–8) will provide three equations for the three unknowns ∇p_j^n, $\nabla \rho_j^n$, and ∇u_j^n. The derivation of the discretization formula will be shown for the interpolation of the primitive variable p, when the Mach number is greater than 1, $M > 1$.

When $M > 1$, the spatial derivatives in Eqs. (6–8) are backward differenced in the standard manner[1] that is used for upwind formulas. The difference equations for the two acoustic equations, Eqs. (7) and (8), can be combined to eliminate ∇u_j^n and obtain an equation for ∇p_j^n. That equation is then used to obtain the formula for the second-order interpolate of p^n at the cell interface located at mesh point $j+1/2$. The second-order interpolate is given by

$$p_{j+1/2}^n = p_j^n + \frac{1}{2}\left(\nabla p_j^n + \tfrac{1}{2}\Delta x \times \left\{\frac{1}{(u+a)_{j-1/2}^n}\left[(p_t)_j + (\rho a)_{j-1/2}^n (u_t)_j\right] + \frac{1}{(u-a)_{j-1/2}^n}\left[(p_t)_j - (\rho a)_{j-1/2}^n (u_t)_j\right]\right\}\right) \tag{9}$$

In Eq. (9), the expression on the right-hand side inside the outermost brackets follows from combining the left-hand sides of the two acoustic equations, Eqs. (7) and (8), to eliminate the term ∇u_j^n. The term ∇p_j^n provides the second-order spatial interpolate and the remaining terms are temporal derivatives that result from combining the acoustic equations. Note that Eq. (9) for p is similar in form to Eq. (5) for u in the case of the linear advection equation. As before, the interpolation formula includes additional terms that involve eigenvalues and temporal derivatives. This appearance of eigenvalues and temporal derivatives in the formulas for higher-order interpolates distinguishes this method from others.

To finish the specification of this formula for interpolation, the discretizations of the time derivatives in Eq. (9) need to be specified. An evaluation of the time derivatives was chosen that uses time levels n and $n-1$, although in Eq. (5) for the advection equation, the time derivative was evaluated by using time levels $n+1$ and n. This explicit evaluation using levels of known data was chosen so that the method could be tested in an existing code by making only minor coding modifications in the MUSCL approach for interpolating the primitive variables[11] p, u, v, and ρ. With that choice, Eq. (9) becomes

$$p_{j+\frac{1}{2}}^n = p_j^n + \tfrac{1}{2}\tilde{\nabla} p_j^n \tag{10}$$

where

$$\tilde{\nabla} p_j^n = \nabla p_j^n + \frac{1}{2}\frac{\Delta x}{\Delta t} \times \left\{ \frac{1}{(u+a)_{j-\frac{1}{2}}^n}\left[(p_j^n - p_j^{n-1}) + (\rho a)_{j-\frac{1}{2}}^n (u_j^n - u_j^{n-1})\right] + \frac{1}{(u-a)_{j-\frac{1}{2}}^n}\left[(p_j^n - p_j^{n-1}) - (\rho a)_{j-\frac{1}{2}}^n (u_j^n - u_j^{n-1})\right] \right\} \tag{11}$$

In Eq. (11), the values of $u+a$ and ρa at the point $j-1/2$ are taken as the average of values at j and $j-1$. The value of $u-a$ at $j-1/2$ is taken as the average of only the nonnegative values at j and $j-1$, plus a small positive term of the order of 10^{-6}. This special evaluation of the term $u-a$ is made to keep its value positive for the numerical stability of the finite differencing. In a steady flow calculation, as the solution approaches convergence, the additional terms in Eq. (11) that approximate time derivatives will vanish. The remaining terms will provide higher-order interpolates without the use of limiter functions and hence produce an accurate resolution of the flow field.

Similar formulas can be derived for higher-order interpolates of u and ρ. For u, the difference equations for Eqs. (7) and (8) are combined to eliminate ∇p_j^n to obtain an expression for ∇u_j^n. Again, time derivatives of p and u will occur in the expression. For ρ, the difference equations for Eqs. (6–8) can be combined to eliminate ∇p_j^n and ∇u_j^n to obtain an equation for $\nabla \rho_j^n$. That expression will include time derivatives of p, u, and ρ.

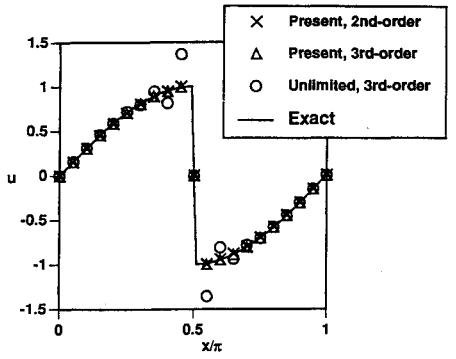

Fig. 1 Solution u of Burger's equation with a source term.

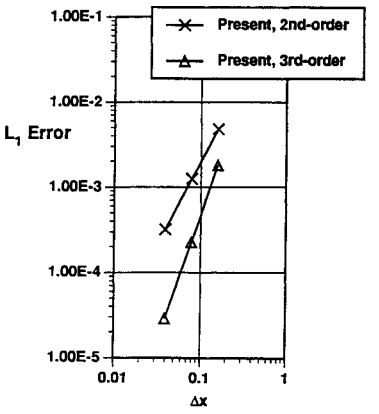

Fig. 2 L_1 error vs mesh spacing.

Next, the formulas need to be extended to situations where there is mixed supersonic and subsonic flow. For a negative eigenvalue, the corresponding time derivative in Eqs. (6–8) is switched from evaluation at mesh point j to $j-1$. This switching is similar to that in first-order, upwind methods, but here the time derivatives are switched in spatial location, rather than the spatial fluxes. For example, in a region of subsonic flow, $M<1$, for which $u>0$, Eq. (11) is changed to

$$\tilde{\nabla} p_j^n = \nabla p_j^n + \frac{1}{2}\frac{\Delta x}{\Delta t}\left\{ \frac{1}{(u+a)_{j-\frac{1}{2}}^n}\left[(p_j^n - p_j^{n-1}) + (\rho a)_{j-\frac{1}{2}}^n (u_j^n - u_j^{n-1})\right] + \frac{1}{(u-a)_{j-\frac{1}{2}}^n}\left[(p_{j-1}^n - p_{j-1}^{n-1}) - (\rho a)_{j-\frac{1}{2}}^n (u_{j-1}^n - u_{j-1}^{n-1})\right] \right\} \tag{12}$$

Now the value of $u-a$ at $j-1/2$ is taken as the average of only the negative values at j and $j-1$, plus a small negative term of the order of 10^{-6}. Again, this special evaluation of the term $u-a$ is made to keep its value negative in this case for the numerical stability of the finite differencing.

At transonic shock waves, the higher-order interpolates are turned off. Those shock waves are detected by the vanishing of an acoustic eigenvalue in a region of compressed flow. The detection algorithm was developed from the one in Ref. 10. For example, Eq. (11) is implemented only if 1) the eigenvalue $u-a$ is positive at grid point j and 2) its average from grid points j and $j+1$ is also positive. The algorithm is looking downstream in supersonic flow to detect the shock wave. Similarly, Eq. (12) is implemented only if 1) the eigenvalue $u-a$ is negative at grid point $j-1$ and 2) its average from grid points $j-1$ and $j-2$ is also negative. Now the algorithm is looking upstream in subsonic flow to detect the shock wave.

Note that higher-order interpolates are not valid at a shock wave since Taylor series expansions do not exist at a discontinuity. However, in this method, across shock waves, the underlying first-order algorithm imposes the Rankine-Hugoniot shock jump relations, which are exact. Again, note that the shock waves are detected by the vanishing of an acoustic eigenvalue. This manner of detection stands in marked contrast to the means that are used by limiter functions or ENO schemes.

At sonic expansion points, an interpolation formula is used that is an average of those that are used at subsonic and supersonic points. For example, the average of Eqs. (11) and (12) is used at points $j-1/2$ if the eigenvalue $u-a$ is positive at points j and $j+1/2$ and negative at $j-1$ and $j-3/2$. Similar formulas are derived when $u<0$.

For third-order accuracy, a standard third-order interpolation formula is used to implement these new formulas. For example, when Eq. (11) is applicable at points j and $j+1$, then

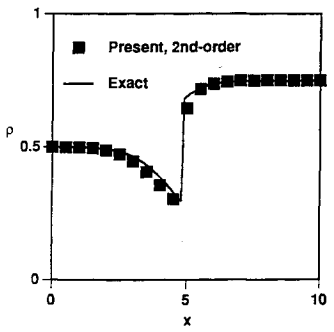

Fig. 3 Density profile. Solution of the Euler equations for flow through a converging-diverging nozzle.

the third-order interpolate for the pressure is given by the standard formula[11]

$$p^n_{j+\frac{1}{2}} = p^n_j + \tfrac{1}{4}\left[(1-\kappa)\tilde{\nabla}p^n_j + (1+\kappa)\tilde{\nabla}p^n_{j+1}\right] \tag{13}$$

with $\kappa = \frac{1}{3}$.

For an extension of this method to multidimensions, either two or three, the compatibility equations are used along the coordinate directions, one at a time, to obtain spatial interpolates along each direction. To obtain compatibility equations along a coordinate direction, the spatial derivatives along the other coordinate directions are dropped from the Euler equations in conservative form. For example in two dimensions, the resulting compatibility equations along the x coordinate direction are given by Eqs. (6-8) and the equation

$$v_t + uv_x = 0 \tag{14}$$

for the component of velocity v along the y coordinate direction. In two dimensions, equations similar to Eqs. (11) and (12) are valid. The only changes are to replace indices for grid locations in one dimension with those for locations in two dimensions. Similarly, the formulas are directly extendible to three dimensions. This extension to multidimensional problems is similar to the method used by the standard, upwind, first-order schemes.

For use with curvilinear coordinates, the compatibility equations are written in curvilinear coordinates. Then the same procedure that was used in the case of Cartesian coordinates to derive Eq. (11), for example, is used to derive a generalized form of Eq. (11).

For viscous flows, the grid was modified to capture the boundary layer and viscous terms[2] were added to the governing equations. However, the same interpolation formulas for higher-order accuracy were used for the convective terms as in the inviscid case; that is, there was no change in the formulas or coding of the convective terms from the inviscid case. The viscous terms were evaluated by using second-order central differencing.

III. Computed Results

In this section, computed results will be presented that have been obtained by using this new algorithm. Solutions to Burger's equation and the Euler and Navier-Stokes equations are shown. For all these results, comparisons[6] with results obtained by using the minmod limiter function indicate that the present method improved the accuracy of the calculations.

Burger's Equation

The first case solves Burger's equation with a source term

$$u_t + (u^2/2)_x = (\sin 2x)/2, \quad u(0) = 0, \quad 0 \le x \le \pi \tag{15}$$

Figure 1 shows results using the new method with second- and third-order accuracy, a result without any dissipation, and the exact solution. The results show that the present method closely matches the exact solution. Figure 2 gives plots of an analysis of the L_1 error of the present method as the grid is refined. The results indicate that the expected orders of accuracy are achieved.

One-Dimensional Euler Equations

The next case solves Euler's equations in one dimension. The flow occurs through a converging and then diverging nozzle. The governing equations are

$$(AQ)_t + (AF)_x = S \tag{16}$$

$$Q = \begin{bmatrix} \rho \\ \rho u \\ e \end{bmatrix}, \quad F = \begin{bmatrix} \rho u \\ \rho u^2 + p \\ (e+p)u \end{bmatrix}, \quad S = \begin{bmatrix} 0 \\ p(\mathrm{d}A/\mathrm{d}x) \\ 0 \end{bmatrix} \tag{17}$$

$$p = (\gamma - 1)(e - \tfrac{1}{2}\rho u^2) \tag{18}$$

$$A = 1.4 + a \times \tanh(0.8x - 4) \tag{19}$$

$$0 \le x \le 10; \quad A = 1, \quad \text{at} \quad x = 0 \tag{20}$$

Figure 3 shows the density profile. Here the first-order, upwind scheme, which was extended to higher order, was Roe's scheme.[1] The comparisons are between the exact solution and the new method. The computed results are second-order accurate. Without the use of any limiting or use of the compatibility equation, the second-order calculations diverged. An analysis of the L_1 error, as the grid was refined, was made for this case. It showed that the new method achieved the expected order of accuracy.

Two-Dimensional Euler and Navier-Stokes Equations

In this section, results will be shown for inviscid and viscous flow over an airfoil. The equations were solved in two dimensions and curvilinear coordinates used. Here a streamwise upwind, first-order algorithm[2] was extended to higher order. The calculations are second-order accurate. The airfoil is NACA 0012. Implicit time marching[12] was used. All the grids used in these calculations were C grids. The grid refinement occurred in the ξ coordinate direction, which is the direction that wraps around the airfoil.

Inviscid Flow, $M_\infty = 0.8$, $\alpha = 1.25$ deg

The first case is that of inviscid flow at Mach number $M_\infty = 0.8$ and the angle of attack of the airfoil occurs at $\alpha = 1.25$ deg. Calculations were made on three successively finer grids;

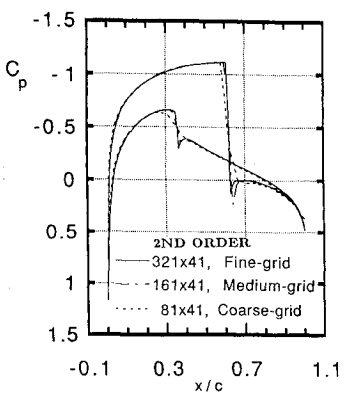

Fig. 4 Pressure coefficients. Inviscid calculations; NACA 0012 airfoil, $M_\infty = 0.8$, $\alpha = 1.25$ deg.

coarse, medium, and fine grids with 81×41, 161×41, and 321×41 grid points, respectively. Figure 4 shows a comparison of pressure coefficients obtained on the three grids. The results are relatively grid-independent, except in the regions of large gradients, which is to be expected from grid refinement. The relative grid independence in the regions of low-flow gradients is an indication that this method is providing an accurate resolution of the flow field.

Next, pressure contours in the field are shown on the medium grid and an extra-fine grid with 161×41 and 321×81 grid points, respectively. The grid points have been doubled in both the directions along the airfoil and normal to it. Figure 5 illustrates pressure contours on the medium grid. In Fig. 5, the weak shock wave on the lower surface is indicated by the clustering of contour lines. Figure 6 shows pressure contours on the extra-fine grid and it shows that the present method has adequately resolved the weak shock and re-expansion region downstream of it.

This transonic case was also computed with Roe's scheme[1] in order to evaluate the dependence of the results on the underlying first-order method. The results were very similar to those shown in Figs. 4–6. Hence, this method of implementing higher-order accuracy can be used with other upwind schemes. Also, this case was computed with a central differencing scheme that used very small amounts of numerical dissipation. Those results were very close to the results from the present method shown in Figs. 4–6. The only difference occurred at the strong shock wave, where the central differencing method showed a preshock overshoot due to the lack of numerical dissipation. Also, this flow case was computed using third-order accurate interpolates with the present method. The results were almost identical to the second-order results expected for minor improvements at the shock waves.

Inviscid Flow, $M_\infty = 1.1$, $\alpha = 0$ deg

The next case is that of inviscid flow at Mach number $M_\infty = 1.1$ and the angle of attack occurs at $\alpha = 0$ deg. Figure 7 shows pressure contours in the field. In this case, the shock waves at the trailing edge of the airfoil are oblique. The large expansion regions in front of the shock waves and large compression region at the leading edge are indications that there is little numerical dissipation with the present method. Comparisons[6] with results obtained by using the minmod limiter function showed an improvement in accuracy with the present method. For the minmod results, the expansion and compression regions were relatively smaller, as they were in the previous case for a subsonic freestream Mach number.

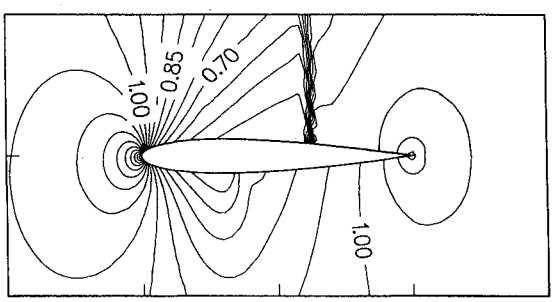

Fig. 5 Pressure contours on the medium grid, 161×41 points. $M_\infty = 0.8$, $\alpha = 1.25$ deg.

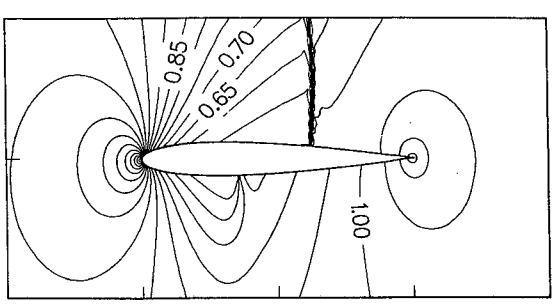

Fig. 6 Pressure contours on the extra-fine grid, 321×81 points. $M_\infty = 0.8$, $\alpha = 1.25$ deg.

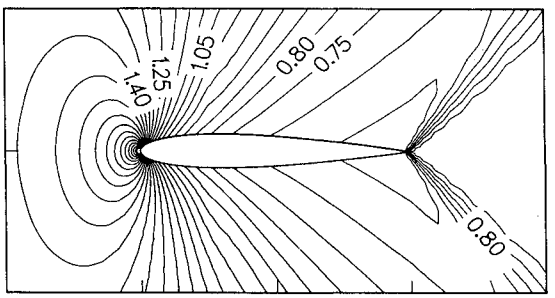

Fig. 7 Pressure contours on the medium grid, 161×41 points. $M_\infty = 1.1$, $\alpha = 0$ deg.

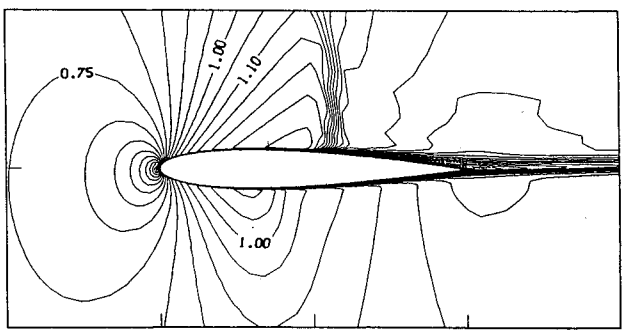

Fig. 8 Mach number contours. Viscous calculations, 81×41 grid points. $M_\infty = 0.8$, $\alpha = 1.25$ deg, $Re = 10^6$.

Viscous Flow, $M_\infty = 0.8$, $\alpha = 1.25$ deg, $Re = 10^6$

The final case is that of viscous flow at Mach number $M_\infty = 0.8$, with an angle of attack at $\alpha = 1.25$ deg and Reynolds number of $Re = 10^6$. The Baldwin-Lomax eddy-viscosity model was used to evaluate the turbulent viscosity coefficient. For the viscous case, the grid spacing in the direction normal to the airfoil was concentrated near the body to capture the boundary layer. At the airfoil, the spacing was reduced by a factor of 100 from that for the inviscid case, from 0.01 to 0.0001 of the chord length. The number of grid points used were 81×41. Figure 8 shows Mach contour plots in the flow field and the resolution of the boundary layer. The calculation of the viscous case provided a test of the stability of the method on a grid with extremely fine spacing. There was no modification of the algorithm or the coding for the convective terms. The only change was to include the viscous terms in the governing equations.

IV. Concluding Remarks

A new method for higher-order accuracy has been developed that uses the compatibility equations. The scheme is philosophically consistent with the underlying, first-order, upwind schemes, which are also based on the compatibility equations. As the results indicate, this method has been successfully applied to the Euler and Navier-Stokes equations. Comparisons[6] of computed results with those obtained by using the

minmod limiter function showed an improvement in accuracy with the present method.

There are several directions for further developments and applications of this scheme. One algorithmic extension would be to develop formulas for the higher-order interpolates by using the compatibility equations along the streamwise[2] direction, rather than coordinate lines. This extension is important because the vanishing of acoustic eigenvalues along coordinate lines does not precisely locate the shock waves. Rather they are located where the total Mach number equals 1. Other algorithmic extensions would be to develop other implementations of the compatibility equations into higher-order interpolates, such as implicit implementations or implementations into interpolates for characteristic variables. Those approaches were used for the linear advection equation, Eq. (5), and also for the transonic, small-disturbance potential equation.[10] Using those approaches for the Euler equations would provide a simple and direct implementation of the compatibility equations for obtaining higher-order interpolates. Further applications could be to viscous flows with vortices, such as supersonic flow over a delta wing at an angle of attack.[2] In those flows, the resolution of the vortices requires either accurate higher-order methods or very fine grids.

Finally, another application could be to unsteady flows, for example, flows about oscillating airfoils or wings.[12] In that application, the temporal derivatives in the interpolates would only be applied in regions of sharp gradients in flow variables, similar in approach to the use of limiter functions.

References

[1]Roe, P. L., "Characteristics-Based Schemes for the Euler Equations," *Annual Review of Fluid Mechanics,* Vol. 18, 1986, pp. 337-365.

[2]Goorjian, P. M., and Obayashi, S., "A Streamwise Upwind Algorithm Applied to Vortical Flow over a Delta Wing," *Proceedings of the 8th GAMM Conference on Numerical Methods in Fluid Mechanics* (Delft, The Netherlands), Sept. 27-29, 1989; also NASA TM 102225, Oct. 1989, and *Notes on Numerical Fluid Mechanics,* Vol. 29, edited by P. Wesseling, Vieweg, 1990.

[3]Harten, A., "Recent Developments in Shock-Capturing Schemes," ICASE Rept. 91-8, Jan. 1991.

[4]Harten, A., "On a Class of High Resolution Total-Variation-Stable Finite-Difference Schemes," *SIAM Journal of Numerical Analysis,* Vol. 21, 1984, pp. 1-23.

[5]Harten, A., and Osher, S., "Uniformly High Order Accurate Nonoscillatory Schemes," *SIAM Journal of Numerical Analysis,* Vol. 2, 1987, pp. 279-309.

[6]Goorjian, P. M., and Obayashi, S., "Higher Order Accuracy by Using the Compatibility Equations for Upwind Algorithms," *Compendium of Abstracts, NASA/AIAA CFD Conference* (NASA Ames Research Center) March 12-14, 1991; also, *Proceedings of the AIAA 10th Computational Fluid Dynamics Conference* (Honolulu, HI), AIAA, Washington, DC, 1991 (AIAA Paper 91-1543).

[7]Van Leer, B., Lee, W. T., and Roe, P., "Characteristic Time-Stepping or Local Preconditioning of the Euler Equations," *Proceedings of the AIAA 10th Computational Fluid Dynamics Conference* (Honolulu, HI), AIAA, Washington, DC, 1991 (AIAA Paper 91-1552).

[8]Lerat, A., and Sides, J., "Implicit Transonic Calculations Without Artificial Viscosity or Upwinding. Numerical Simulation of Compressible Euler Flows," *Notes on Numerical Fluid Dynamics,* Vol. 26, Vieweg, 1989.

[9]Pulliam, T. H., and Steger, J. L., "Recent Improvements in Efficiency, Accuracy, and Convergence for Implicit Approximate Factorization Algorithms," AIAA Paper 85-360, Jan. 1985.

[10]Goorjian, P. M., and Van Buskirk, R., "Second-Order-Accurate Spatial Differencing for the Transonic Small-Disturbance Equation," *AIAA Journal,* Vol. 23, No. 11, 1985, p. 1693; also AIAA Paper 84-0091, AIAA 22nd Aerospace Sciences Meeting (Reno, NV), Jan. 9-12, 1984.

[11]Anderson, W. K., Thomas, J. L., and van Leer, B., "Comparison of Finite Volume Flux Vector Splittings for the Euler Equations," *AIAA Journal,* Vol. 24, No. 9, 1986, pp. 1453-1460.

[12]Obayashi, S., Guruswamy, G. P., and Goorjian, P. M., "Streamwise Upwind Algorithm for Computing Unsteady Transonic Flows Past Oscillating Wings," *AIAA Journal,* Vol. 29, No. 10, 1991, pp. 1668-1677; also Errata, *AIAA Journal,* Vol. 30, No. 2, 1992, p. 569.